AD-A091 820 PENNSYLVANIA STATE UNIV UNIVERSITY PARK APPLIED RESE--ETC F/G 20/4
AN AXISYMMETRIC, STRONG-INTERACTION PROCEDURE TO INCLUDE LARGE,--ETC(U)
JUL 80 M S DIETZ N00024-79-C-6043
UNCLASSIFIED ARL/PSU/TM-80-160 NL

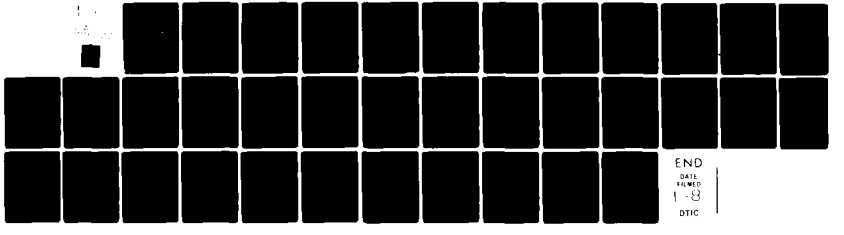

END
DATE FILMED
1-81
DTIC

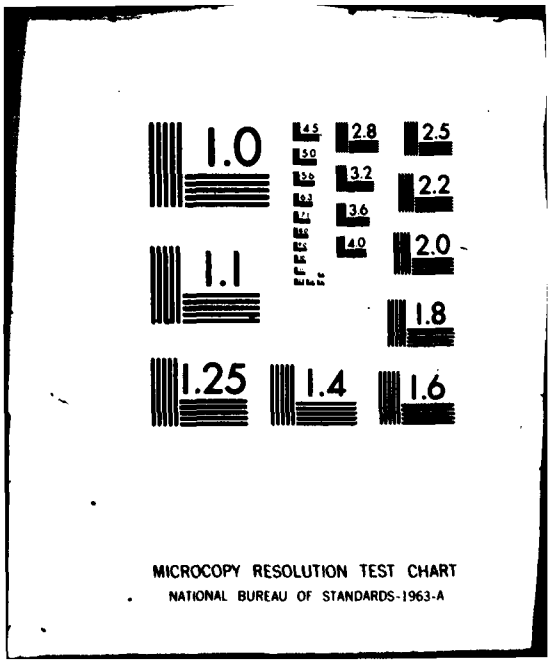
1.0
1.1
1.25
1.4
1.6
1.8
2.0
2.2
2.5
2.8
3.2
3.6
4.0
4.5
5.0
5.6
6.3
7.1
MICROCOPY RESOLUTION TEST CHART
NATIONAL BUREAU OF STANDARDS-1963-A

AN AXISYMMETRIC, STRONG-INTERACTION PROCEDURE TO INCLUDE LARGE, NORMAL PRESSURE GRADIENTS

M. S. Dietz

Technical Memorandum
File No. 80-160
24 July 1980
Contract No. N00024-79-C-6043
Copy No. 31

The Pennsylvania State University
APPLIED RESEARCH LABORATORY
Post Office Box 30,
State College, Pa. 16801

NAVY DEPARTMENT
NAVAL SEA SYSTEMS COMMAND

UNCLASSIFIED
SECURITY CLASSIFICATION OF THIS PAGE (When Data Entered)

REPORT DOCUMENTATION PAGE

READ INSTRUCTIONS BEFORE COMPLETING FORM

1. REPORT NUMBER: ARL/PSU/TM-80-160	2. GOVT ACCESSION NO.: AD-A091 820
3. RECIPIENT'S CATALOG NUMBER	
4. TITLE (and Subtitle): An Axisymmetric, Strong-Interaction Procedure to Include Large, Normal Pressure Gradients	5. TYPE OF REPORT & PERIOD COVERED: Technical Memorandum
6. PERFORMING ORG. REPORT NUMBER	
7. AUTHOR(s): M. S. Dietz	8. CONTRACT OR GRANT NUMBER(s): N00024-79-C-6043
9. PERFORMING ORGANIZATION NAME AND ADDRESS: Applied Research Laboratory, Post Office Box 30, State College, Pa. 16801	10. PROGRAM ELEMENT, PROJECT, TASK AREA & WORK UNIT NUMBERS
11. CONTROLLING OFFICE NAME AND ADDRESS: Naval Sea Systems Command, Washington, DC 20362 Code NSEA-63R-31	12. REPORT DATE: 24 July 1980
	13. NUMBER OF PAGES: 32
14. MONITORING AGENCY NAME & ADDRESS(if different from Controlling Office)	15. SECURITY CLASS. (of this report): Unclassified
	15a. DECLASSIFICATION/DOWNGRADING SCHEDULE

16. DISTRIBUTION STATEMENT (of this Report)

Approved for Public Release.Distribution Unlimited Per NAVSEA-October 28, 1980.

17. DISTRIBUTION STATEMENT (of the abstract entered in Block 20, if different from Report)

18. SUPPLEMENTARY NOTES

19. KEY WORDS (Continue on reverse side if necessary and identify by block number)

flow, axisymmetric, boundary layer, pressure, gradient

20. ABSTRACT (Continue on reverse side if necessary and identify by block number)

This report presents a modified strong-interaction procedure for axisymmetric bodies. The modifications include the addition of the normal momentum equation to the boundary-layer calculations and the patching of the viscous-inviscid flow solutions at the boundary-layer edge to account for large, normal pressure gradients. The resulting weakly elliptic problem is solved by an iterative technique. Based on results to date, the use of an under-relaxation factor and some smoothing are required to obtain a converged solution.

DD FORM 1 JAN 73 1473 EDITION OF 1 NOV 65 IS OBSOLETE

UNCLASSIFIED
SECURITY CLASSIFICATION OF THIS PAGE (When Data Entered)

Subject: An Axisymmetric, Strong-Interaction Procedure to Include Large, Normal Pressure Gradients

References: See page 22.

Abstract: This report presents a modified strong-interaction procedure for axisymmetric bodies. The modifications include the addition of the normal momentum equation to the boundary-layer calculations and the patching of the viscous-inviscid flow solutions at the boundary-layer edge to account for large, normal pressure gradients. The resulting weakly elliptic problem is solved by an iterative technique. Based on results to date, the use of an under-relaxation factor and some smoothing are required to obtain a converged solution.

Acknowledgements: The author greatly appreciates the advice and criticism of Dr. Gilbert H. Hoffman. This work is sponsored by the Naval Sea Systems Command, Code NSEA-63R-31.

TABLE OF CONTENTS

LIST OF FIGURES

NOMENCLATURE

C_p - static pressure coefficient = $\dfrac{p^* - p_\infty^*}{\frac{1}{2}\rho^* U_\infty^{*2}}$

C_{p_δ} - static pressure coefficient at the boundary-layer edge = $\dfrac{p_\delta^* - p_\infty^*}{\frac{1}{2}\rho^* U_\infty^{*2}}$

p - static pressure = $\dfrac{p^*}{\rho^* U_\infty^{*2}}$

p_δ - static pressure at the boundary-layer edge = $\dfrac{p_\delta^*}{\rho^* U_\infty^{*2}}$

r - distance normal from centerline = $\dfrac{r^*}{L^*}$

r_o - body radius = $\dfrac{r_o^*}{L^*}$

Re - Reynolds number = $\dfrac{\rho^* U_\infty^* L^*}{\mu^*}$

u - velocity component in x-direction = $\dfrac{u^*}{U_\infty}$

u_e - velocity component in x-direction at the boundary-layer edge = $\dfrac{u_e^*}{U_\infty}$

v - velocity component normal to the body surface = $\dfrac{v}{U_\infty}$

v_e - velocity component normal to the body surface at the boundary-layer edge = $\dfrac{v_e}{U_\infty}$

Nomenclature (cont.)

$-\overline{u'v'}$ Reynolds stress in the boundary layer $= \dfrac{-\rho^* \overline{(u'v')}}{\rho^* U_\infty^{*2}}$

x - arc length distance along body $= \dfrac{x^*}{L^*}$

y - distance normal to body surface $= \dfrac{y^*}{L^*}$

ε - turbulent eddy viscosity $= \dfrac{\rho^* \varepsilon^*}{\mu^*}$

ϕ - body surface angle, see Figure 2

ψ - Stokes stream function $= \dfrac{\psi^*}{\rho^* L^{*2} U_\infty^*}$

ψ_δ - Stokes stream function at the boundary-layer edge $= \dfrac{\psi_\delta^*}{\rho^* L^{*2} U_\infty^*}$

τ - shear stress $= \dfrac{\tau^*}{\rho^* U_\infty^{*2}}$

All of the above definitions are nondimensional and based on the following dimensional reference quantities.

L^* - reference length

μ^* - dynamic viscosity

ρ^* - density

τ^* - shear stress

U_∞^* - free stream velocity

INTRODUCTION

1.1 Origin and Importance of the Investigation

In dealing with the flow field around axisymmetric bodies, difficulties arise in the vicinity of the tail. Here the thickness of the boundary layer produces a displacement effect, altering the inviscid pressure distribution. The resultant curvature of the outer streamlines causes the development of a significant normal pressure gradient across the boundary layer, thus negating the thin layer approximation currently used to calculate boundary layer flow. This is the so-called strong-interaction region, named for the strongly coupled turbulent and inviscid flow that exists at the aft end of the body. The accuracy of the prediction of the flow field in this area is important due to its major contribution to the total flow drag.

Present treatment of the strong-interaction phenomenon involves the simultaneous solution of the equations governing the boundary layer and inviscid flow fields using a displacement body technique. The procedure is iterative. The viscous flow is calculated using a pressure distribution determined from inviscid flow theory. The displacement thickness is calculated and added to the original body. This displacement body is then used to calculate a new inviscid pressure distribution and the cycle is repeated until convergence. An example of this method is presented by Hoffman [1]*.

1.2 Statement of the Problem

In the correct application of the displacement body method the normal pressure gradient is accounted for by mapping the pressure distribution of the displacement body back to the original body while conserving the arc length. Whether or not this properly models the strong-interaction flow has become a point of contention [2]. By directly including the normal pressure gradient the accuracy of the flow field prediction should be improved.

The mechanics of this problem requires the coupling of the normal momentum equation to the streamwise momentum equation and the continuity equation. All simplifications with regard to the pressure terms in these equations are dropped. As in the displacement body technique, the simultaneous solution of viscous and inviscid equations involves an iterative procedure, but there are two major differences. First, the potential flow solution is patched to the edge of the boundary layer rather than the displacement body. Second, the pressure variation through the boundary layer is calculated at each station in the flow using the edge pressure determined from the potential flow.

---

*Numbers in brackets designate References at the end of report.

The final results will be the prediction of the pressure distributions on the body, at the edge of the boundary layer and wake, and along the wake centerline. Once these values are known, conventional methods can be employed to calculate the important flow parameters, including the drag coefficient of the body.

1.3 General Scope of the Investigation

The subject of the investigation is the F-57 Body examined by Patel and Lee [3], shown in Figure 1. This body was chosen for several reasons, most important of which is its cusped tail. The cusp allows the boundary-layer calculations to continue smoothly into the wake without the discontinuity that would accompany a finite-angle tail. Also, the large amount of experimental data already available on the F-57 Body makes it an excellent subject for the initial testing of a numerical procedure. After obtaining a converged solution for the simplified case, the method could be extended to include finite-angle tails. Due to insufficient time, that problem was not addressed in this report.

THEORETICAL DEVELOPMENT

2.1 Boundary Layer Theory

The boundary layer equations for a body of revolution, considering only incompressible, steady flow, are [4]:

$$\text{Continuity:}\quad \frac{\partial}{\partial x}(ru) + \frac{\partial}{\partial y}(rv) = 0 \quad , \tag{1}$$

$$\text{X-Momentum:}\quad u\frac{\partial u}{\partial x} + v\frac{\partial u}{\partial y} = -\frac{\partial p}{\partial x} + \frac{1}{r}\frac{\partial}{\partial y}\left[r\left(\frac{1}{Re}\frac{\partial y}{\partial y} - \overline{u'v'}\right)\right] \quad , \tag{2}$$

$$\text{Y-Momentum:}\quad u\frac{\partial v}{\partial x} + v\frac{\partial v}{\partial y} = -\frac{\partial p}{\partial y} \quad , \tag{3}$$

where all variables are dimensionless. The coordinate system employed is shown in Figure 2 as it applies to the aft portion of the body. From Figure 2, the relationship between r and y is

$$r(x,y) = r_o(x) + y\cos\phi \tag{4}$$

Equations (1) - (3) include the assumption that all the stress terms in the original Navier-Stokes equations, except the σ_{xy} gradient, are negligibly small. They do not, however, allow for the pressure gradient normal to the surface to go to zero. The boundary conditions are:

$$u(x,0) = 0 \quad , \tag{5}$$

$$v(x,0) = 0 \quad , \tag{6}$$

$$\lim_{y\to\infty} u(x,y) = u_e(x) \quad . \tag{7}$$

The Reynolds stress is related to the velocity field by assuming the relationship

$$\overline{-u'v'} = \frac{\varepsilon}{Re} \frac{\partial u}{\partial y} \tag{8}$$

where ε is the eddy viscosity. Using Equation (7), the x-momentum equation becomes

$$u \frac{\partial u}{\partial x} + v \frac{\partial u}{\partial y} = - \frac{\partial p}{\partial x} + \frac{1}{rRe} \frac{\partial}{\partial y} \left[r(1 + \varepsilon) \frac{\partial u}{\partial y} \right] \quad . \tag{9}$$

At this point, the equations must be put into a form compatible with the existing ARL boundary layer program in scaled physical variables, which employs Keller's Box Method. The Reynolds number is eliminated from the streamwise momentum equation by introducing the following scaled variables:

$$v = \frac{\bar{v}}{\sqrt{Re}} \quad , \tag{10}$$

$$y = \frac{\bar{y}}{\sqrt{Re}} \quad . \tag{11}$$

Equations (1), (2), and (3) respectively

$$\frac{\partial}{\partial x} (ru) + \frac{\partial}{\partial y} (r\bar{v}) = 0 \quad , \tag{12}$$

$$u \frac{\partial u}{\partial x} + v \frac{\partial u}{\partial \bar{y}} = \frac{\partial p}{\partial x} + \frac{1}{r} \frac{\partial}{\partial \bar{y}} \left[r(1 + \varepsilon) \frac{\partial u}{\partial \bar{y}} \right] \quad , \tag{13}$$

$$u \frac{\partial \bar{v}}{\partial x} + v \frac{\partial \bar{v}}{\partial y} = - Re \frac{\partial p}{\partial \bar{y}} \quad , \tag{14}$$

In order to use the box method, the Stokes stream function is introduced to manipulate the equations into the necessary first-order form. The scaled Stokes stream function is defined as

$$ru = \frac{\partial \psi}{\partial \bar{y}} \quad , \quad r\bar{v} = - \frac{\partial \psi}{\partial x} \tag{15}$$

Equation (12) is identically satisfied by the stream function. Grouping terms and defining the laminar shear stress as

$$\tau = \frac{\partial u}{\partial \bar{y}} \tag{16}$$

and

$$b = (1 + \epsilon) \tag{17}$$

the streamwise momentum equation, Equation (13), can be written in first-order form,

$$\frac{r}{2}\frac{\partial}{\partial x}(u^2 + 2p) - \frac{\partial \psi}{\partial x}\tau - \frac{\partial}{\partial \bar{y}}(rb\tau) = 0 \quad . \tag{18}$$

The first-order set of equations to be solved is:

$$\frac{\partial}{\partial \bar{y}}(rb\tau) = \frac{r}{2}\frac{\partial}{\partial x}(u^2 + 2p) - \frac{\partial \psi}{\partial x}\tau \tag{19}$$

$$\frac{\partial u}{\partial \bar{y}} = \tau \tag{20}$$

$$\frac{\partial \psi}{\partial \bar{y}} = ru \tag{21}$$

$$\frac{1}{2}\frac{\partial(\bar{v}^2)}{\partial \bar{y}} + Re\,\frac{\partial p}{\partial y} = -u\frac{\partial \bar{v}}{\partial x} \tag{22}$$

The boundary conditions for this set of equations are:

$$u = \bar{v} = \psi = 0 \qquad \text{at } \bar{y} = 0 \tag{23}$$

$$u \to u_e \qquad \text{at } \bar{y} \to \infty \tag{24}$$

$$\tau = 0 \qquad \text{at } \bar{y} = 0 \text{ (only in wake)} \tag{25}$$

Equations (19) - (21) form the conventional, parabolic set of boundary-layer equations. The addition of Equation (22), however, couples this set to the elliptic, potential flow equations. Fortunately, this coupling is weak, thus allowing the normal momentum equation to lag one cycle in an iterative calculation scheme.

2.2 Eddy Viscosity Model

The algebraic eddy viscosity model used in the boundary-layer calculations is a modification of the Baldwin-Lomax turbulence model [6], [7]. It consists of an inner (law of the wall) and outer (law of the wake) region defined as follows:

$$\text{Inner Region:} \quad \varepsilon_i = Re^{3/2}\, \ell^2\, |\tau| \tag{26}$$

where

$$\ell = \text{mixing length} = 0.41\, \bar{y}\, [1 - \exp(-y^+/A^+)] \tag{27}$$

A^+ = flat plate damping length constant = 26.0

$$y^+ = \text{Reynolds number based on the friction velocity} = \frac{u_\tau y}{\nu} \tag{28}$$

$$u_\tau = \text{friction velocity} = (\tau_w/p)^{1/2} \tag{29}$$

Normally, the damping length constant is a function of the pressure gradient at the wall, $(\partial p/\partial x)_w$. Due to the present method of calculation, inclusion of this term presents difficulties that are too time-consuming to be considered for this report.

$$\text{Outer Region:} \quad \varepsilon_0 = Re\, K\, C_{cp}\, F_{KLEB}\,(y)\, F_{wake} \tag{30}$$

where

K = Clauser constant - 0.0168

$C_{cp} = 1.60$

$$F_{wake} = \begin{cases} \bar{y}_{max}\, F_{max}\, Re^{-1/2} \\ 0.25\, \bar{y}_{max}\, u^2_{DIF}\, Re^{1/2}/F_{max} \end{cases} \quad \text{the smaller}$$

F_{max} and u_{DIF} are determined from

$$F(\bar{y}) = \bar{y}\ |\tau|\ [1 - \exp\ (-y^+/A^+)] \tag{31}$$

and

$$u_{DIF} = u_{MAX} - u_{MIN} \tag{32}$$

$$F_{KLEB}(y) = \text{Klebanoff intermittancy} = [1 + 5.5\ (\bar{y}\ 0.3/y_{max})^6]^{-1} \tag{33}$$

NUMERICAL METHODS

As stated earlier, the final set of boundary-layer equations is only weakly elliptic. The normal momentum equation can then be uncoupled, leaving the conventional boundary-layer equations which are solved by a marching technique. The calculation of the normal pressure gradient becomes an extra step in the strong-interaction procedure, lagging one cycle in the iteration. The other major modification to the procedure is the patching of the boundary-layer and potential-flow solutions at the boundary-layer edge instead of matching them at the displacement body surface. The numerical and computational methods required to institute these changes, including smoothing and under-relaxation, will be discussed in the following sections.

3.1 Boundary-Layer and Potential-Flow Programs

The two major programs employed are a boundary-layer program and an inviscid-flow program. The boundary-layer program used was developed by Hoffman [8] and is similar in method to that presented by Cebeci and Smith [9]. It is a general finite-difference solution of the incompressible boundary-layer equations on a body of revolution based on the Keller Box Method. The program is written in physical variables, necessitating the input of a starting profile as a singularity is encountered at the body nose in this formulation. It does, however, allow for calculations to proceed uninterrupted into the wake, a requirement in this elliptic problem to correctly predict the flow at the aft end of the body. Programs using the Mangler transformation employ an integral method into the wake due to a singularity at the tail. This would not be conducive to the present investigation because discrete values of the flow parameters are required throughout the boundary-layer and wake flows for use in subsequent normal pressure calculations. The program is capable of treating laminar or turbulent flow up to a separation point and includes transverse curvature effects. Major modifications to the program included:

A. Reformulation of the boundary-layer equations in terms of the pressure and addition of a subroutine that calculates the pressure variation across the boundary layer at each station. The pressure gradient is determined by applying a two-point-backwards finite-difference method to the normal momentum equation and using values of u and $\bar{v}$ saved from the previous iteration.

B. Calculation of the normal component of the velocity at each station using a two-point-backwards, finite-difference method. This includes the input of two profiles from the program in Mangler-Levy-Lees variables.

C. Addition of a subroutine that calculates the boundary-layer thickness δ at the point in the flow where $u = 0.995\ u_e$. Values of the stream function and radius are then determined at $y = \delta$. These values define the so-called "displaced, leaky body," a pseudo-body consisting of the physical body with the boundary-layer thickness added with flow through its "walls" from boundary-layer entrainment. The leaky body is used as input to the potential flow program.

D. Addition of a subroutine that changes the axial step size from a variable to a constant value and interpolates for ψ_δ and r_δ at the new locations.

The inviscid-flow program was also developed by Hoffman [5]. It involves the frozen vorticity equations for axisymmetric flow formulated using a spline-relaxation technique. The Douglas-Neumann program for inviscid flow was a possible option and in fact is used to obtain the initial distribution. Hoffman's program is used in preference for later iterations due to its availability and the ease with which it could be modified to meet the needs of the present investigation. Input to the program includes an initial profile in spline variables and the "leaky body" information. The C_p distribution at δ is then calculated by sweeping from left to right in the streamwise direction and performing line relaxation at each station until a converged solution is obtained. The only modifications to the program involved elimination of a junction region between body and wake calculations that was made irrelevant by the cusped tail on the F-57 body. One limitation imposed by this program was that the input data must be in constant increments in the axial direction. This was accomplished by taking the variable step size data, fitting it with cubic splines, and interpolating for new values with a constant increment.

Assorted auxillary programs are used between runs of the two main programs to examine, compare, and smooth data. Cubic splines are employed in accomplishing the latter with manual control over the choice of the spline nodes.

3.2 Solution of the Normal Momentum Equation

The final form of the normal momentum equation expressed in Eq. (22) was

$$\frac{1}{2}\frac{\partial(\bar{v}^2)}{\partial y} + Re\,\frac{\partial p}{\partial y} = -\,u\,\frac{\partial \bar{v}}{\partial x} \quad .$$

The first attempt at numerical solution of this equation employed the Keller box method, the basis for the conventional boundary layer portion of the program. This formulation was abandoned without a test run when an oscillation appeared in the calculation of $\bar{v}$ which employed the same method. In order to avoid these oscillations, which seem to be inherent in the box method, the derivative of the normal velocity component with respect to x was computed using a second-order, finite-difference method with a variable step size. The general form of this equation is

$$f'_{i+1} = \frac{\frac{\Delta x_1}{\Delta x_2}\left(f_{i-1} - f_i\right) - \left(\frac{\Delta x_2}{\Delta x_1} + 2\right)\left(f_{i+1} - f_i\right)}{\Delta x_1 + \Delta x_2} \qquad (34)$$

where f is the variable in question, i - 1, i, and i + 1 are three consecutive stations, and Δx_1 and Δx_2 are the steps in x between the stations. Centering the normal momentum equation of i + 1 and j + 1/2, then using standard central differences for the y-derivatives gives the following result:

$$\frac{1}{2}\left[\frac{\bar{v}^2_{j+1} - \bar{v}^2_{j}}{\Delta \bar{y}_j}\right]_{i+1} + Re\left[\frac{p_{j+1} - p_j}{\Delta \bar{y}_j}\right]_{i+1} + \left[\frac{\left(u\frac{\partial \bar{v}}{\partial x}\right)_{j+1} - \left(u\frac{\partial \bar{v}}{\partial x}\right)_{j}}{2}\right]_{i+1} = 0 \; . \qquad (35)$$

Equation (35) is then solved downwards from the boundary-layer edge employing a given edge pressure and known velocity profiles. The equation's final form, with the i + 1 subscript understood, is

$$p_j = p_{j+1} + \frac{1}{2Re}\left(\bar{v}^2_{j+1} - \bar{v}^2_{i+1}\right) + \frac{\Delta \bar{y}_j}{2Re}\left[\left(u\frac{\partial \bar{v}}{\partial x}\right)_{j+1} + \left(u\frac{\partial \bar{v}}{\partial x}\right)_{j}\right] \quad . \qquad (36)$$

Equation (36) is allowed to lag one cycle in the iterative procedure. Values of u and $\bar{v}$ are saved from the boundary-layer run and are used with the newly calculated edge pressure from the inviscid program to calculate the pressure variation through the boundary layer in the next iteration. The values of u are determined as one of the variables in the conventional boundary layer calculations. The method for calculating $\bar{v}$ will be considered next.

3.3 Normal Velocity Calculations

The variation of the normal component of velocity through the boundary layer is obtained by solving for $\bar{v}$ from the continuity equation. An alternate solution involving the definition of the Stokes stream function,

$$\bar{v} = -\frac{1}{r}\frac{\partial \psi}{\partial x} \quad , \tag{37}$$

was eventually used as a consistency check, but the continuity formulation was preferred due to the ease with which it could be extended beyond the boundary-layer edge. Beginning with the continuity equation, we have

$$\frac{\partial}{\partial x}(ru) + \frac{\partial}{\partial \bar{y}}(r\bar{v}) = 0 \quad . \tag{38}$$

As stated earlier, the use of the Keller box method in solving this equation resulted in oscillations in the profiles from station to station. The problem was resolved, as in the pressure calculation, by using backward differences for the derivatives in the x-direction and then centering along a vertical element of the boundary-layer grid. The resulting equation, solved for $(r\bar{v})_{j+1}$ at station i + 1, is

$$(r\bar{v})_{j+1} = (r\bar{v})_j - \frac{\delta \bar{y}_j}{2}\left[\frac{\partial}{\partial x}(ru)_{j+1} + \frac{\partial}{\partial x}(ru)_j\right] \quad . \tag{39}$$

Equation (39) is solved from the body surface, where $\bar{v}_j = 0$, upwards to the boundary-layer edge.

3.4 Determination of the Boundary-Layer Edge and Associated Values

The boundary-layer and inviscid-flow solutions are patched together at the boundary-layer edge in the present calculation. Therefore the location of the boundary-layer edge and the values of several parameters at the edge must be determined. The values of the radius and Stokes stream function at δ are required as input to the potential-flow program. $\bar{v}_e$ is also needed to calculate u_e in the next iteration of the boundary-layer program. It is desirable to have these distributions as smooth as possible when first calculated to reduce the amount of manual smoothing required. Several methods of determining the boundary layer were explored

and abandoned due to unsatisfactory results. Each will be briefly described with the results, which led to the best choice, shown in terms of ψ_δ and r_δ in Figure 3.

The initial procedure was simply to allow the parameters to be defined at the last point in the boundary-layer calculation at each station. Due to the nature of these calculations, specifically the choppy growth pattern of the boundary-layer "edge," the results are very ragged and therefore highly unsatisfactory.

The next method involved evaluation of δ at the $\bar{y}$ value where $u = 0.995\ u_e$. The interpolation was accomplished with cubic splines. This approximate boundary-layer edge was then used to determine r_δ, ψ_δ, and $\bar{v}_e$ by a similar interpolation. This method resulted in a relatively smooth distribution except where oscillations in u occurred. Note that these oscillations occur in the tail region of the body. The fluctuations again make this method undesirable.

The final method was to input a fixed, smooth curve as the boundary-layer edge. The curve was initially determined by taking the output from the second method and manually smoothing it with a cubic-spline routine. Figure 4 shows the boundary-layer edge determined in this way. It is input into every iteration of the boundary-layer program and the values of r_δ, ψ_δ, and $\bar{v}_e$ are calculated at the corresponding point in the flow.

The results were generally very good. Examining Figure 5, it can be seen that each distribution is at least as smooth as the curve used for interpolation. This method allows for ease in patching the potential and boundary-layer solutions at the boundary-layer edge. It has been suggested [10], however, that the approximated boundary-layer edge may have to be revised in later iterations.

3.5 Calculations Beyond the Boundary-Layer Edge

The box method employed in the boundary-layer program requires the extension of the boundary-layer edge when the value of the shear stress increases over some cutoff value. The nature of the normal velocity and pressure calculations requires that there be grid points and associated values for two stations immediately behind the station in question. Thus, when the boundary-layer edge is extended at station $i + 1$, $\bar{v}$ and p must be obtained beyond the boundary layer at stations i and $i - 1$.

First of all, the simplifying assumption that

$$u = u_e \text{ for } \bar{y} \geq \delta \tag{40}$$

is made. Then $\bar{v}$ can be determined from the continuity equation where

$$\frac{\partial}{\partial \bar{y}} (r\bar{v}) = - \frac{\partial}{\partial x} (ru) = - \frac{\partial}{\partial x} (ru_e) \quad . \tag{41}$$

Integrating Equation (41) from $\bar{y}_j$ to $\bar{y}_{j+1}$ and using the definition of r(x), we obtain the final form of the equation:

$$(r\bar{v})i,j+1 = (r\bar{v})i,j - \left[\alpha(x_i) + \frac{\beta(x_i)}{\sqrt{Re}} \left(\frac{\bar{y}_{j+1} + \bar{y}_j}{2} \right) \right] \Delta y_j \quad , \tag{42}$$

where

$$\alpha(x_i) = \frac{\partial}{\partial x} (u_e \, r_o(x)) \quad ,$$

$$\beta(x_i) = \frac{\partial}{\partial x} (u_e \cos\phi(x)) \quad ,$$

$$\Delta y_j = \bar{y}_{j+1} - \bar{y}_j \quad .$$

$\bar{v}$ can be determined directly from Equation (42) as the value of $r_{i,j+1}$ is known.

Since we are above the boundary-layer edge and in potential flow, Bernoulli's equation holds. Written dimensionally, it is

$$p^* + \frac{1}{2} \rho^* V^{*2} = \text{constant} = c_1 \tag{43}$$

If we define dimensionless variables as follows:

$$\left.\begin{aligned} p^* &= \rho^* U_\infty^{*2} \, p \quad , \\ V^* &= U_\infty^* V \quad , \end{aligned}\right\} \tag{44}$$

then Equation (43) in dimensionless form is

$$p + \frac{1}{2} V^2 = \frac{c_1}{\rho^* U_\infty^{*2}} = c_2 \quad . \tag{45}$$

The constant c_2 can be evaluated at the boundary layer edge as follows:

$$c_2 = p_e + \frac{1}{2} (u_e^2 + v_e^2) \quad . \tag{46}$$

Writing Equation (45) for a point above the boundary-layer edge and substituting Equation (46) for c_2 we have

$$p + \frac{1}{2}(u_e^2 + v^2) = p_e + \frac{1}{2}(u_e^2 + v_e^2) \quad . \tag{47}$$

Solving for p and rewriting in terms of the scaled velocity, $\bar{v}$, we have finally

$$p_{i,j+1} = p_{e_i} + \frac{1}{2Re}(\bar{v}_{e_i}^2 - \bar{v}_{i,j+1}^2) \tag{48}$$

The value of the pressure above the boundary layer can now be calculated employing the value of $\bar{v}_{i,j+1}$ determined from Equation (42).

3.6 Calculation Loops

With the equations and boundary conditions as specified in section 2, the boundary layer calculations proceed as follows:

1. Given $C_{p\delta}$ at station x_i, the normal momentum equation is solved downwards to the body using the values of $u(x,y)$ and $\bar{v}(x,y)$ from the previous iteration. The first iteration is obtained by assuming that $\partial p/\partial y = 0$.

2. Holding $\partial p/\partial y$ fixed, the conventional boundary layer equations are solved from which values of ψ_δ and r_δ are determined.

3. The normal velocity profile, $\bar{v}(x,y)$ is calculated and stored along with the streamwise velocity profile for use in the next iteration.

4. Steps (1 - 3) are repeated, marching downstream until the desired flow field is obtained.

Both the normal and streamwise components of velocity must be stored in two-dimensional arrays. The necessary storage can be minimized by including the pressure calculation only where the normal pressure gradient is significant. This portion of the flow field is from about 70% of the body length onwards, as can be seen in Figure 8. Present calculations were carried out beginning at about 26% of the body length as a test of the accuracy of the method. There should be very little variation between the results using the present method and those using the conventional method (which neglects normal pressure gradient variations) for this early region.

The calculation loop for the entire modified strong-interaction procedure is:

a. Determine an initial guess for $C_p(x)$, including into the wake region.

b. Compute the boundary-layer flow with $\partial p/\partial y = 0$, giving $\delta(x)$, $r_\delta(x)$, and $\psi_\delta(x)$. This effectively defines the "leaky body." Values of $\overline{v}(x,y)$ and $u(x,y)$ are determined and stored for the next iteration.

c. Calculate $C_{p\delta}(x)$ from the "leaky body" inviscid solution.

d. Compute the boundary layer flow, calculating the normal pressure variation at each station using $C_{p\delta}(x)$ determined in step (c) and the velocity profiles from previous iterations. With the values of $\delta(x)$, determined in step (b), calculate new values of $\psi_\delta(x)$ and $r_\delta(x)$.

e. Repeat steps (c) and (d) until convergence is achieved.

A flow chart of the procedure is presented in Figure 6.

3.7 Smoothing and Under-Relaxation

The numerical representation of distinct values of $C_{p\delta}$ and ψ_δ requires some care as the boundary-layer and inviscid-flow solutions depend on the streamwise derivatives of these quantities. Oscillations in either would be amplified and propagated through succeeding calculations. It should be noted, however, that the inviscid-flow formulation being used in this investigation is less sensitive to variations in ψ than conventional programs. Some smoothing of these and other calculated values seems to be in order.

Significant effort was expended to obtain relatively smooth primary output as described in Section 3.4 for the boundary-layer edge calculation. The amount of extra smoothing between programs has so far been restricted to the values of $C_{p\delta}$ from the potential-flow program because its x-wise stations do not coincide with those of the boundary-layer program.

A sweep-to-sweep under-relaxation factor of 0.3 applied to $\overline{v}$ and $C_{p\delta}$ has been suggested by Mahgoub and Bradshaw [10]. As will be shown in the following sections, a value of 0.1 seems to be more appropriate for the first few iterations. Convergence should be at least monotonic and could possibly be improved by increasing the under-relaxation factor for later iterations [10].

RESULTS AND DISCUSSION

4.1 Verification of Computational Methods

Validity checks were made on the newly developed components of the strong-interaction procedure. Both main programs delivered accurate results when run as conventional programs, that is, with all modifications turned off. Then the two major additions, the calculation of $\overline{v}$ and p through the boundary layer, were checked for consistency.

Calculations of $\bar{v}$ using the continuity equation were checked against calculations of $\bar{v}$ using the definition of the stream function,

$$\bar{v} = -\frac{1}{r}\frac{\partial \psi}{\partial x} \quad .$$

The difference between values obtained from the two methods was less than 0.2%. Further, upon comparing results of the present calculation with the theoretical values obtained by Patel and Lee [3], it was found that both methods provide similar profiles, but they are much too full. The ratio of $\bar{v}_{exp}$ to $\bar{v}_{theor}$ in both cases is approximately

$$\frac{\bar{v}_{exp}}{\bar{v}_{theor}} = 0.6$$

as can be seen in Figure 7. Each calculation was made with $\partial p/\partial y = 0$. Better normal velocity profiles should be obtained in later iterations of the present procedure when the pressure is varied through the boundary layer.

The method of determining the normal pressure gradient was also checked. The profiles obtained corresponded to experimental values up to about 70% of the body length. At this point, the values of $\bar{v}$ and $\partial\bar{v}/\partial x$ employed in the normal momentum equation both become much larger than experimental measurements indicate. Consequently, the pressure calculations from this point on are inaccurate and resulting profiles do not agree with experimental values. Resolution of this difficulty is the major stumbling block left in the investigation and is the target of present attempts at under-relaxation and smoothing.

The ability of the patched viscous-inviscid solution to correctly predict the edge pressure was examined next. The experimental values of C_p at the wall were used as input data to the boundary-layer program. Values of C_{p_δ} corresponding to experimental measurements were the expected output from the potential-flow program. Results are shown in Figure 8. The pressure distribution obtained follows the experimental data very closely, even modeling the dip in the tail region. The calculated values are slightly lower than experiment in this region, probably due to the boundary-layer edge approximation employed.

One result that appeared to be incorrect was the dip that occurs at about 80-95% of the body length in the curve of ψ_δ vs. x_B as shown in Figure 5. The curve follows a smooth, increasing trend everywhere except in this area and the fluctuation is not reflected in any of the other boundary-layer parameters. The validity of this dip was checked in the following manner.

The rate of change of the stream function with respect to x at the boundary layer edge can be written as

$$\left(\frac{d\psi}{dx}\right)_\delta = \left(\frac{\partial\psi}{\partial x}\right)_\delta + \left(\frac{\partial\psi}{\partial y}\right)_\delta \left(\frac{dy}{dx}\right)_\delta \tag{49}$$

From the definition of the stream function we have

$$\bar{v}_e = -\left(r\,\frac{\partial\psi}{\partial x}\right)_\delta \qquad u_e = \left(r\,\frac{\partial\psi}{\partial y}\right)_\delta \tag{50}$$

Substituting Equation (50) into Equation (49) we obtain

$$\frac{d\psi_\delta}{dx} = -\frac{\bar{v}_e}{r_\delta} + \frac{u_e}{r_\delta}\left(\frac{d\bar{y}}{dx}\right)_\delta \quad . \tag{51}$$

Equation (51) allows a direct examination of the slope of the curve of ψ_δ and insight into the validity of the dip. All values on the right-hand-side of the equation are output from the boundary-layer program. Magnitudes of the terms can be obtained from Figures 4, 5, and 9. It can be seen that the normal component of the velocity $\bar{v}_e$ increases rapidly to a peak at approximately 90% of the body length, while at the same point r_δ decreases to its lowest value for the rear portion of the body. From the plot of δ, the boundary-layer thickness, we can see that $(d\bar{y}/dx)_\delta$ is constant in the vicinity of the tail of the body. The value of u_e decreases as the flow approaches the aft end of the body. The combined effect points to a decreasing $d\psi_\delta/dx$ over the range from 80% to 90% and gives a plausible explanation to the dip in ψ_δ that occurs in this area.

Overall, the findings of these tests have strengthened the basis for this investigation. They have proven that the pressure distribution can be calculated accurately at the boundary-layer edge, allowing for the patching of the viscous-inviscid flow solutions there. They have shown that the normal velocity and pressure variation through the boundary layer can be calculated. Most importantly, they point the way for the additional numerical experimentation required to overcome current difficulties.

4.2 Convergence

A converged pressure distribution is the ultimate goal of the investigation. To achieve this, several problems must be resolved. By examining Figure 10, it is seen that the $C_{p_{wall}}$ distribution used as a "first guess" for the boundary-layer program differs greatly from the experimental values. This results in the profiles of $\bar{v}_e$ being too full at the tail, as shown in Figure 7, and the large over-correction in C_{p_δ} obtained from the inviscid flow program as seen in Figure 10.

Two basic difficulties in the problem are the extreme sensitivity of the calculations at the tail and the oscillations in u in this region. The flow field changes very rapidly due to the large, streamline curvature at the tail. Small errors in the calculations tend to be magnified thus producing poor convergence characteristics. To minimize the change, under-relaxation factors on the order of 0.1 seem to be called for in the calculation of the normal-velocity and normal-pressure distributions in the first few iterations. The oscillations in u at the tail of the body are inherent in the present physical variable finite difference formulation of the boundary-layer program. Hopefully, they will be smoothed out as the iteration cycle proceeds and the flow field model becomes more precise.

Stated simply, the ultimate convergence of the present investigation depends heavily on the successful application of under-relaxation techniques.

4.3 Conclusions

A method for including the normal pressure gradient in the axisymmetric, strong-interaction calculations has been presented. The determination of the pressure variation through the boundary layer via solution of the normal momentum equation and the patching of the boundary-layer and potential flow solutions at the boundary-layer edge are the major innovations. The procedure was applied to the F-57 body, a low-drag body of revolution with a cusped tail. A converged solution has not been achieved as of this writing. Sensitivity of the calculations along with the large error in the initial pressure profile have limited success in this direction. Current research into the problem is centered around under-relaxation techniques. Proper application of these techniques should result in a converged solution.

The viability of the method has been at least partially established by several of the tests conducted, thus creating a basis for further investigation. Continued research should produce a more accurate means of modeling the flow field at the aft end of a body of revolution.

REFERENCES

1. Hoffman, G. H., "A Modified Displacement Body Method for Treating the Axisymmetric Strong Interaction Problem," Journal of Ship Research, 24, 114, 1980.

2. Nakayama, A., Patel, V. C., and Landweber, L., "Flow Interaction Near the Tail of a Body of Revolution, Part 2: Iterative Solution for Flow Within and Exterior to Boundary Layer and Wake," ASME Journal of Fluids Engineering, Paper No. 76-FE-N, June 17, 1976.

3. Patel, V. C., and Lee, Y. T., "Thick Axisymmetric Turbulent Boundary Layer and Near Wake of a Low-Drag Body of Revolution," Iowa Institute of Hydraulic Research Report No. 210, December 1977.

4. Cebeci, T., and Bradshaw, P., Momentum Transfer in Boundary Layers, (Hemisphere Publishing Corp.), Washington, 1977.

5. Hoffman, G. H., "A Spline Relaxation Procedure for Calculating Axisymmetric Flow Fields About Body/Propeller Combinations; I. Frozen Vorticity and Potential Flows," ARL TM 80-108, 14 May 1980, The Pennsylvania State University, Applied Research Laboratory.

6. Cebeci, T., "Eddy Viscosity Distribution in Thick Axisymmetric Boundary Layers," Journal of Fluids Engineering, 95, 319, 1973.

7. Baldwin, B. S., and Lomax, H., "Thin Layer Approximation and Algebraic Model for Separated Turbulent Flows," AIAA 16th Aerospace Sciences Meeting, Huntsville, AL, January 1978.

8. Hoffman, G. H., Unpublished work.

9. Cebeci, T., and Smith, A. M. O., Analysis of Turbulent Boundary Layers, (Academic Press, New York, 1974).

10. Mahgoub, H. E. H., and Bradshaw, P., "Calculation of Turbulent-Inviscid Flow Interactions with Large Normal Pressure Gradients," AIAA Journal Volume 17, No. 10, October 1979.

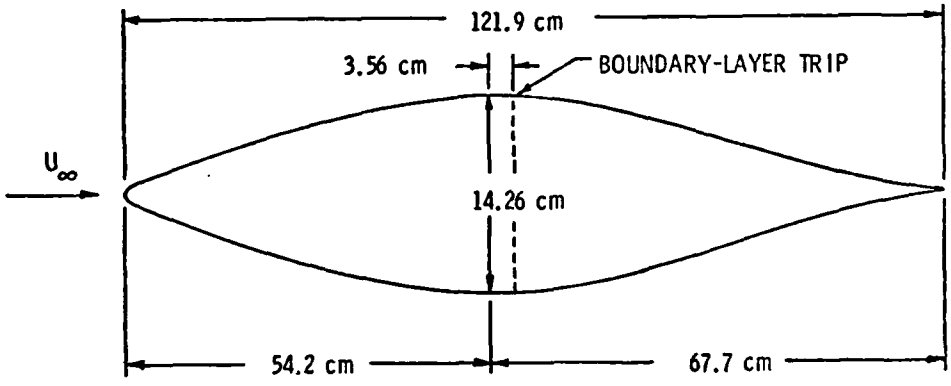

Figure 1. F-57 Body Geometry (Patel and Lee 1977)

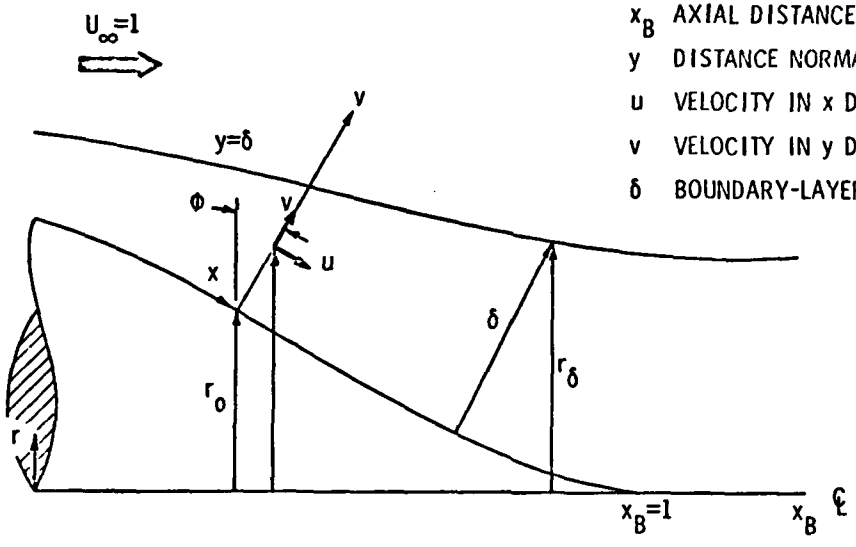

Φ BODY SURFACE ANGLE
r DISTANCE FROM CENTERLINE
r_o BODY RADIUS
x ARC LENGTH ALONG BODY
x_B AXIAL DISTANCE
y DISTANCE NORMAL TO BODY SURFACE
u VELOCITY IN x DIRECTION
v VELOCITY IN y DIRECTION
δ BOUNDARY-LAYER THICKNESS

Figure 2. Definition Sketch of a Cusp-Tailed Body of Revolution.

24 July 1980
MSD:cag

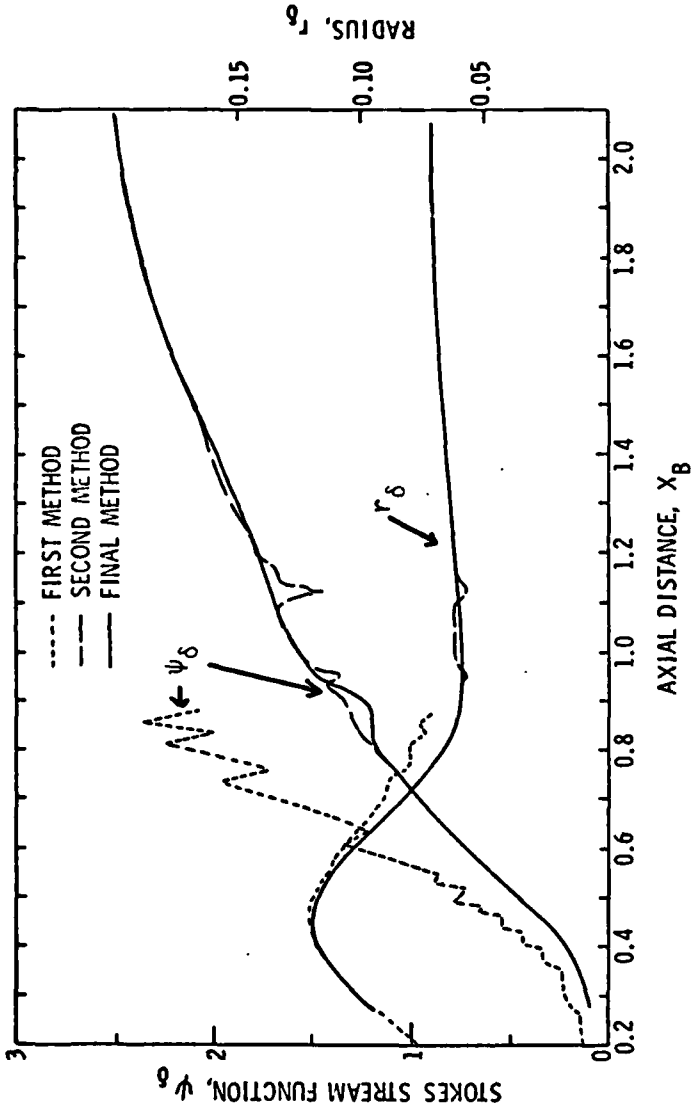

Figure 3. Comparison of Methods for Determining Parameters at the Boundary-Layer Edge.

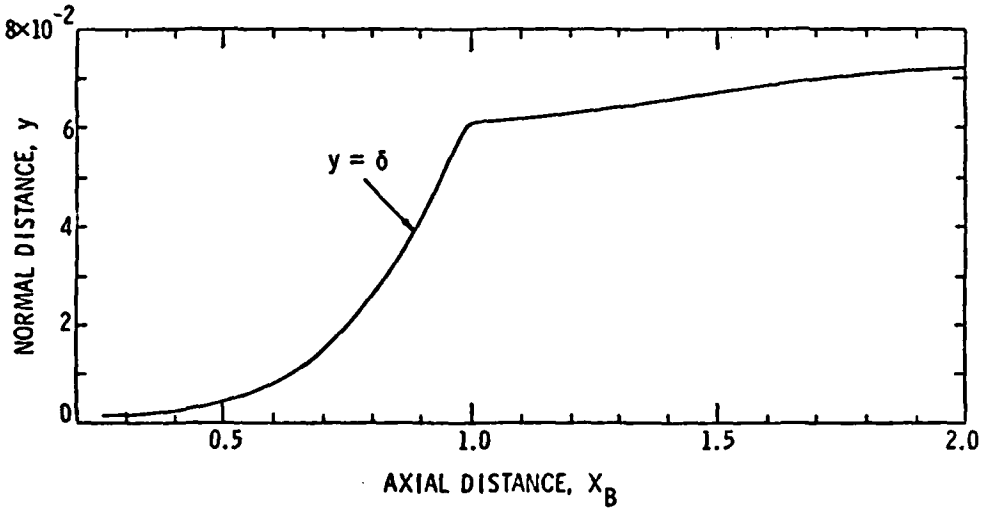

Figure 4. Boundary-Layer Thickness, F-57 Body.

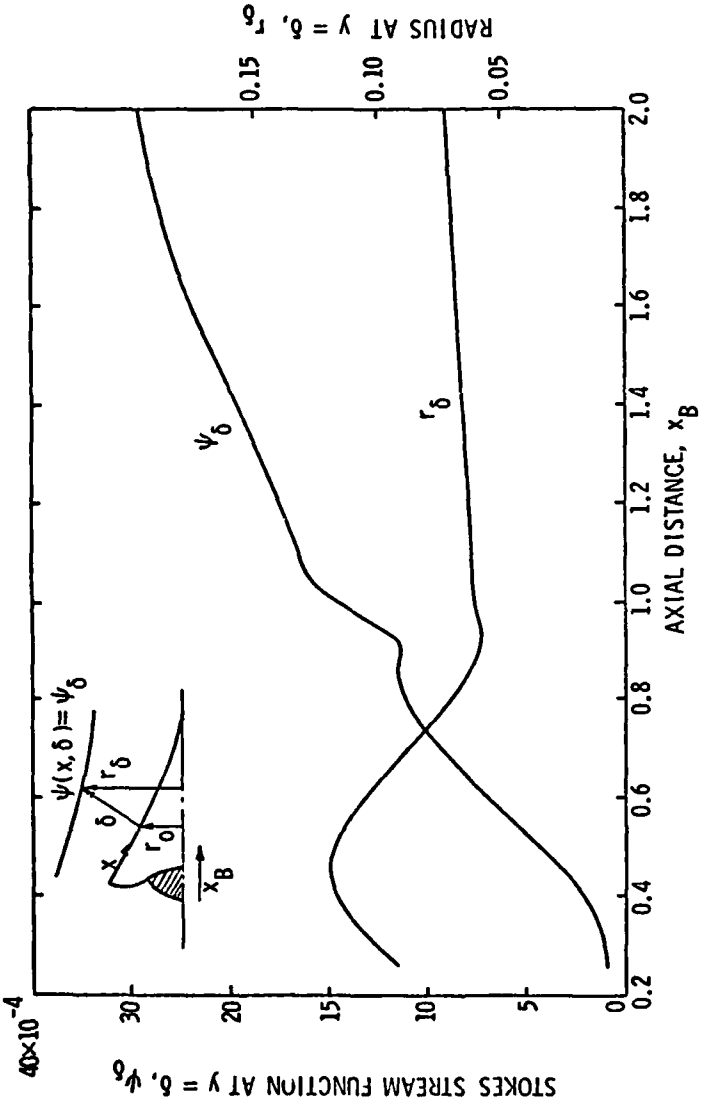

Figure 5. Stokes Stream Function and Radius at the Boundary-Layer Edge, F-57 Body.

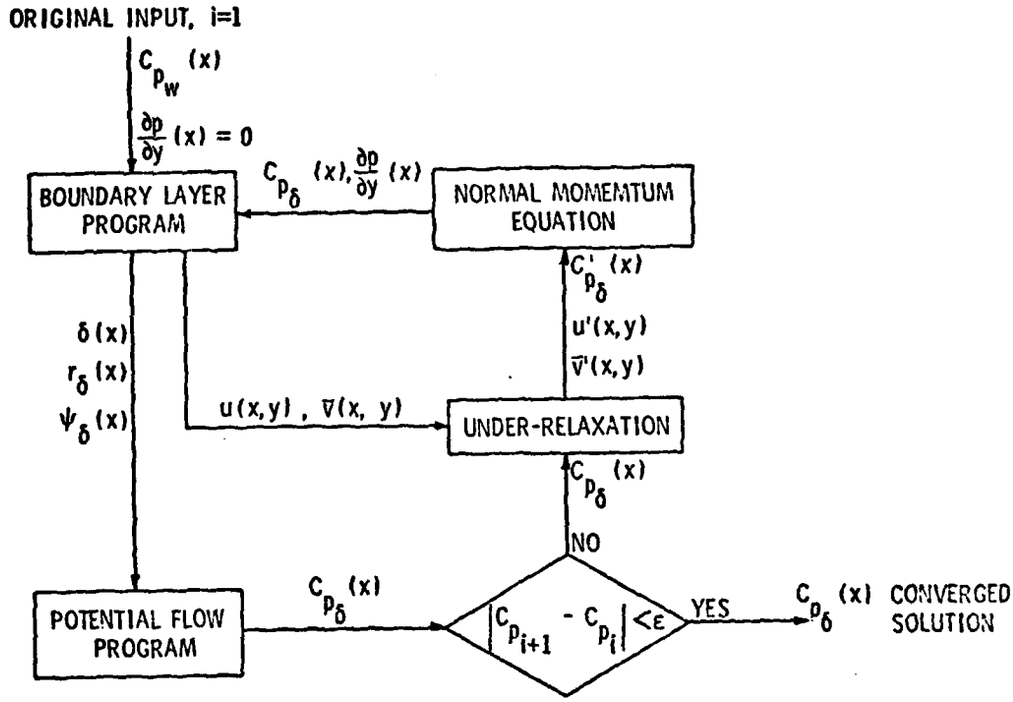

Figure 6. Interaction Scheme for the Modified Strong-Interaction Method.

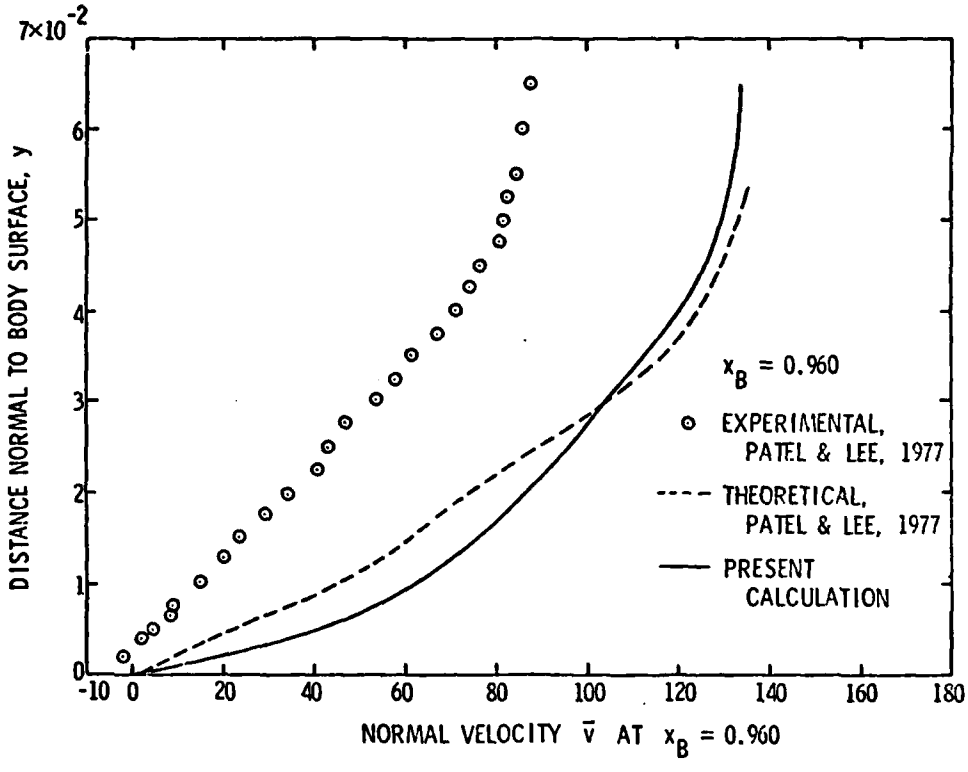

Figure 7. Normal Velocity Profile at $x_B = 0.960$, F-57 Body.

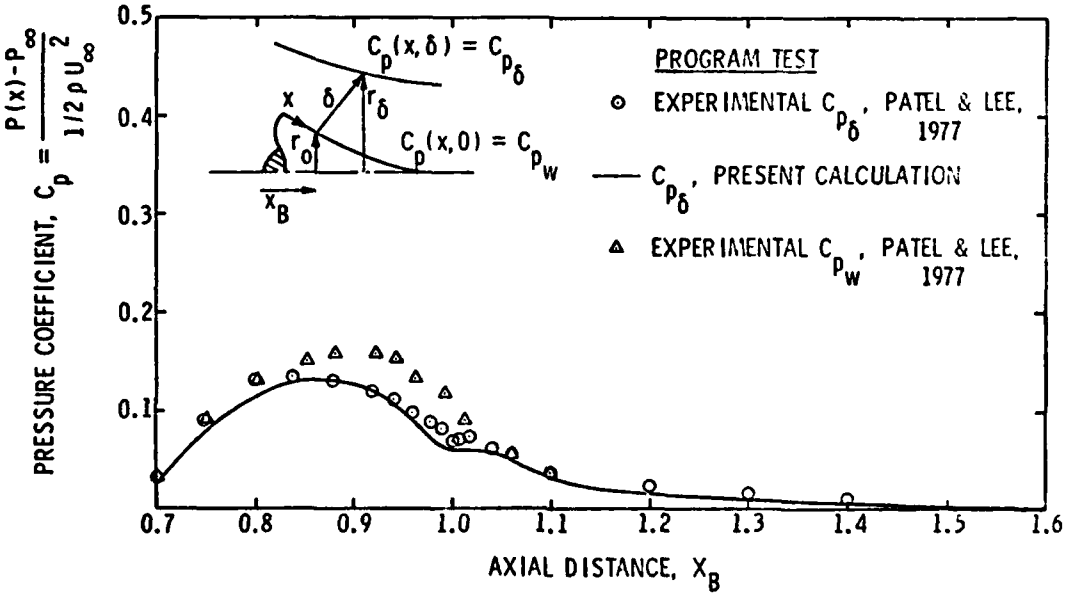

Figure 8. Program Test: C_p Distributions, F-57 Body.

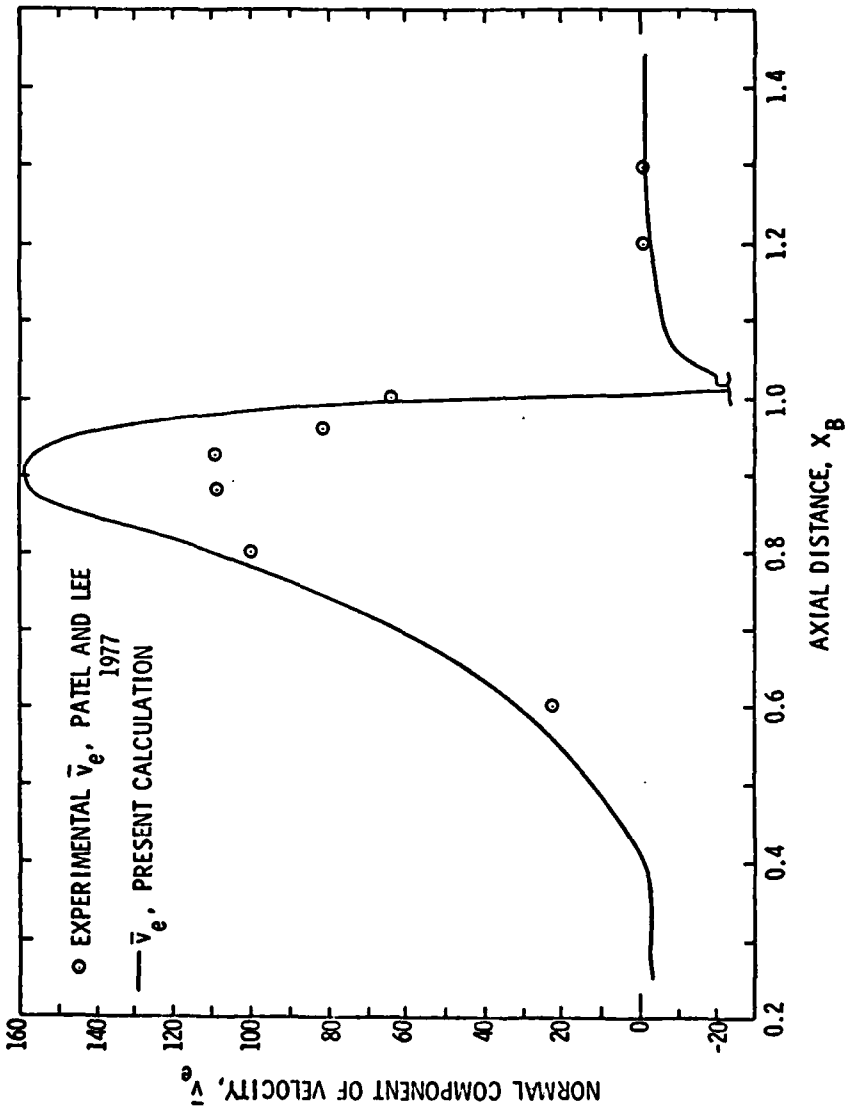

Figure 9. Normal Component of Velocity at the Boundary-Layer Edge, F-57 Body.

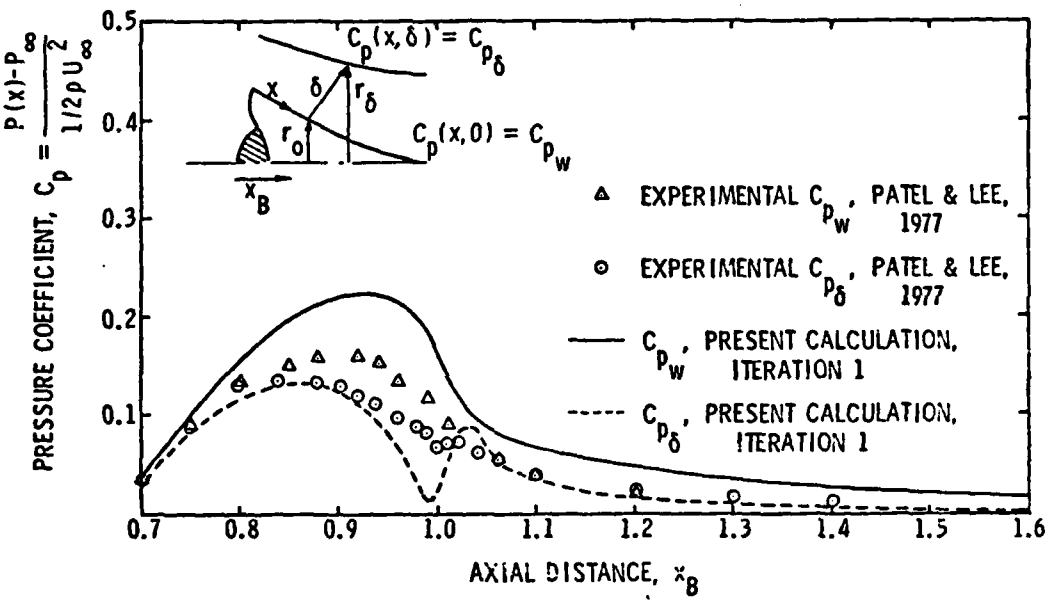

Figure 10. Comparison of C_p on the Body and at the Boundary-Layer Edge, F-57 Body.

DISTRIBUTION LIST FOR UNCLASSIFIED TM 80-160 by M. S. Dietz, dated 24 July 1980

Commander
Naval Sea Systems Command
Department of the Navy
Washington, DC 20362
Attn: Library
Code NSEA-09G32
(Copy Nos. 1 and 2)

Naval Sea Systems Command
Attn: C. G. McGuigan
Code NSEA-63R2
(Copy No. 3)

Naval Sea Systems Command
Attn: E. G. Liszka
Code NSEA-63R1
(Copy No. 4)

Naval Sea Systems Command
Attn: G. Sorkin
Code NSEA-05R
(Copy No. 5)

Naval Sea Systems Command
Attn: T. E. Peirce
Code NSEA-63R-31
(Copy No. 6)

Naval Sea Systems Command
Attn: J. G. Juergens
Code NSEA-05H
(Copy No. 7)

Naval Sea Systems Command
Attn: H. C. Claybourne
Code NSEA-05H5
(Copy No. 8)

Naval Sea Systems Command
Attn: A. R. Paladino
Code NSEA-05H1
(Copy No. 9)

Naval Sea Systems Command
Attn: F. J. Welling
Code NSEA-521
(Copy No. 10)

Commanding Officer
Naval Underwater Systems Center
Newport, RI 02840
Attn: C. N. Pryor
Code 01
(Copy No. 11)

Naval Underwater Systems Center
Attn: D. Goodrich
Code 36301
(Copy No. 12)

Naval Underwater Systems Center
Attn: R. H. Nadolink
Code 3634
(Copy No. 13)

Naval Underwater Systems Center
Attn: R. Trainor
Code 36314
(Copy No. 14)

Naval Underwater Systems Center
Attn: F. White
Code 36314
(Copy No. 15)

Naval Underwater Systems Center
Attn: Library
Code 54
(Copy No. 16)

Commanding Officer
Naval Ocean Systems Center
San Diego, CA 92152
Attn: D. Nelson
Code 6342
(Copy No. 17)

Commanding Officer and Director
David W. Taylor Naval Ship R&D Center
Department of the Navy
Bethesda, MD 20084
Attn: W. B. Morgan
Code 15
(Copy No. 18)

David W. Taylor Naval Ship R&D Center
Attn: R. Cumming
Code 1544
(Copy No. 19)

David W. Taylor Naval Ship R&D Center
Attn: T. T. Huang
Code 1552
(Copy No. 20)

David W. Taylor Naval Ship R&D Center
Attn: J. McCarthy
Code 154
(Copy No. 21)

DISTRIBUTION LIST FOR UNCLASSIFIED TM 80-160 by M. S. Dietz, dated 24 July 1980

David W. Taylor Naval Ship R&D Center
Attn: M. Sevik
Code 19
(Copy No. 22)

David W. Taylor Naval Ship R&D Center
Attn: Library
Code 522
(Copy No. 23)

Commanding Officer and Director
David W. Taylor Naval Ship R&D Center
Department of the Navy
Annapolis Laboratory
Annapolis, MD 21402
Attn: J. G. Stricker
Code 2721
(Copy No. 24)

Commander
Naval Surface Weapons Center
Silver Spring, MD 20910
Attn: G. C. Gaunaurd
Code R-31
(Copy No. 25)

Naval Surface Weapons Center
Attn: J. L. Baldwin
Code WA-42
(Copy No. 26)

Naval Surface Weapons Center
Attn: W. J. Glowacki
Code R-44
(Copy No. 27)

Naval Surface Weapons Center
Attn: J. M. Solomon
(Copy No. 28)

Office of Naval Research
Department of the Navy
800 N. Quincy Street
Arlington, VA 22217
Attn: R. Cooper
Code 438
(Copy No. 29)

Office of Naval Research
Attn: H. Fitzpatrick
Code 438
(Copy No. 30)

Defense Technical Information Center
5010 Duke Street
Cameron Station
Alexandria, VA 22314
(Copy Nos. 31 to 42)

National Bureau of Standards
Aerodynamics Section
Washington, DC 20234
Attn: P. S. Klebanoff
(Copy No. 43)

Rand Corporation
1700 Main Street
Santa Monica, CA 90406
Attn: C. Gazley
(Copy No. 44)

California Institute of Technology
Jet Propulsion Laboratory
4800 Oak Grove Drive
Pasadena, CA 91103
Attn: Dr. Leslie Mack
(Copy No. 45)

Iowa Institute of Hydraulic Research
The University of Iowa
Iowa City, Iowa 52240
Attn: V. C. Patel
(Copy No. 46)

Dynamics Technology, Inc.
3838 Carson Street, Suite 110
Torrance, CA 90503
Attn: Wayne H. Haigh
(Copy No. 47)

The Pennsylvania State University
Applied Research Laboratory
Post Office Box 30
State College, PA 16801
Attn: J. J. Eisenhuth
(Copy No. 48)

Applied Research Laboratory
Attn: R. E. Henderson
(Copy No. 49)

Applied Research Laboratory
Attn: G. H. Hoffman
(Copy No. 50)

DISTRIBUTION LIST FOR UNCLASSIFIED TM 80-160 by M. S. Dietz, dated
24 July 1980

Applied Research Laboratory
Attn: Garfield Thomas Water Tunnel Files
(Copy No. 51)